# Electric-Field Dependent Decays of Two Spectroscopically Different M-States of Photosensory Rhodopsin II from *Natronobacterium pharaonis*

Laura Rivas,* Silke Hippler-Mreyen,† Martin Engelhard,† and Peter Hildebrandt*‡
*Instituto de Tecnologia Química e Biológica, Universidade Nova de Lisboa, P-2781-901 Oeiras, Portugal;
†Max-Planck-Institut für Molekulare Physiologie, D-44227 Dortmund, Germany; and
‡Technische Universität Berlin, Institut f. Chemie, D-10623 Berlin, Germany

ABSTRACT Sensory rhodopsin II (NpSRII) from *Natronobacterium pharaonis* was studied by resonance Raman (RR) spectroscopic techniques. Using gated 413-nm excitation, time-resolved RR measurements of the solubilized photoreceptor were carried out to probe the photocycle intermediates that are formed in the submillisecond time range. For the first time, two M-like intermediates were identified on the basis of their C=C stretching bands at 1568 and 1583 $cm^{-1}$, corresponding to the early $M(L)_{400}$ state with a lifetime of 30 $\mu$s and the subsequent $M(1)_{400}$ state with a lifetime of 2 ms, respectively. The unusually high C=C stretching frequency of $M(1)_{400}$ has been attributed to an unprotonated retinal Schiff base in a largely hydrophobic environment, implying that the $M(L)_{400} \rightarrow M(1)_{400}$ transition is associated with protein structural changes in the vicinity of the chromophore binding pocket. Time-resolved surface enhanced resonance Raman experiments of NpSRII electrostatically bound onto a rotating Ag electrode reveal that the photoreceptor runs through the photocycle also in the immobilized state. Surface enhanced resonance Raman spectra are very similar to the RR spectra of the solubilized protein, ruling out adsorption-induced structural changes in the retinal binding pocket. The photocycle kinetics, however, is sensitively affected by the electrode potential such that at 0.0 V (versus Ag/AgCl) the decay times of $M(L)_{400}$ and $M(1)_{400}$ are drastically slowed down. Upon decreasing the potential to −0.4 V, that corresponds to a decrease of the interfacial potential drop and thus of the electric field strength at the protein binding site, the photocycle kinetics becomes similar to that of NpSRII in solution. The electric-field dependence of the protein structural changes associated with the M-state transitions, which in the present spectroscopic work is revealed on a molecular level, appears to be related to the electric-field control of bacteriorhodopsin's photocycle, which has been shown to be of functional relevance.

## INTRODUCTION

Bacteria have evolved intricate mechanisms to respond adequately and efficiently to environmental challenges. Archaea like *Halobacterium salinarum* or *Natronobacterium pharaonis* can react toward chemical stimuli as well as toward light. The latter input signal triggers a phototactic transduction pathway which is mediated by two receptors, sensory rhodopsin I (SRI) and sensory rhodopsin II (SRII), which are responsible for directing the bacteria toward favorable light conditions (Spudich and Luecke, 2002; Spudich, 1998; Schäfer et al., 1999). SRI and SRII are structurally closely related to each other and to the two other archaeal rhodopsins, the ion pumps bacteriorhodopsin (BR) and halorhodopsin (HR). All four archaeal pigments contain an all-*trans* retinal bound to the seven-helix membrane protein via a protonated Schiff base. Whereas BR, HR, and SRI absorb at wavelengths above 560 nm, SRII from *H. salinarum* has its absorption maximum at around 490 nm. On excitation by light the archaeal rhodopsins undergo characteristic photoreaction cycles, which are coupled to the physiological response, i.e., signal transduction or ion pumping. Sensory rhodopsins from *H. salinarum* have been sequenced (Blanck et al., 1989; Zhang et al., 1996) and in the case of the photophobic receptor also from the phylogenetically distinct *N. pharaonis* (NpSRII) (Seidel et al., 1995). The biochemical and physiological properties of NpSRII are quite similar to those of SRII from *H. salinarum*, as demonstrated in measurements of the photocycle (Scharf et al., 1992).

The photocycle of NpSRII, which has been investigated in a number of studies (Chizhov et al., 1998; Hirayama et al., 1992; Miyazaki et al., 1992; Imamoto et al., 1992), is quite similar to that of BR (Lanyi and Váró, 1995), except that the turnover is slowed down by about two orders of magnitude. Recent work (Chizhov et al., 1998) has shown that the photocycle follows a scheme of irreversible first-order reactions connecting kinetically distinct protein states ($P_i$; I=1,2,..8). These states are formed from five spectrally distinct species ($S_i$), namely $NpSRII_{510}$ ($K_{510}$), $NpSRII_{495}$ ($L_{495}$), $NpSRII_{400}$ ($M_{400}$), $NpSRII_{485}$ ($N_{485}$), and $NpSRII_{535}$ ($O_{535}$). On light excitation of the retinylidene chromophore isomerization of all-*trans* → 13-*cis* occurs, which is followed by thermal relaxations via the archetypical intermediates K, L, M, N, and O back to the original ground state. Accompanying these transitions are proton transfer steps which lead to vectorial proton transfer to the extracellular medium (Schmies et al., 2001). Whereas the first part

*Submitted October 25, 2002, and accepted for publication January 22, 2003.*

Address reprint requests to Peter Hildebrandt, Tel.: +49-30-314-21419; Fax: +49-30-314-21122; E-mail: hildebrandt@chem.tu-berlin.de.



0006-3495/03/06/3864/10 $2.00

of the photocycle can be readily explained by the reaction sequence

$$\mathrm{NpSRII}_{500}(\mathrm{P}_0) \overset{h\nu}{\Rightarrow} \mathrm{K}_{510}(\mathrm{P}_1) \rightarrow \mathrm{L}_{495}(\mathrm{P}_2) \rightarrow [\mathrm{L}_{495} \Leftrightarrow \mathrm{M(L)}_{400}](\mathrm{P}_3) \rightarrow \mathrm{M(1)}_{400}(\mathrm{P}_4) \rightarrow \mathrm{M(2)}_{400})(\mathrm{P}_5) \Rightarrow \ldots,$$

the second part in which the ground state is re-formed is more complicated as it comprises fast equilibria between the M, N, and O spectral states.

According to this model, the M spectral states are contained in three different protein states ($P_3$, $P_4$, $P_5$) which will be denoted M(L), M(1), and M(2), respectively. In the photocycle of BR the spectrally silent transition between $M_1$ and $M_2$ ($P_4 \rightarrow P_5$) has been correlated to a switch, which alters the accessibility of the Schiff base from the extracellular side to the cytoplasmic side, hence guaranteeing the vectorial transport of protons. A similar protein conformational change, the outward movement of helix F, has also been shown to occur in NpSRII (Wegener et al., 2000).

Vibrational spectroscopy of NpSRII revealed considerable conformational movement already at the early stages of the photocycle (Kandori et al., 2001; Engelhard et al., 1996). The $L \rightarrow M$ transition is accompanied by the protonation of Asp-75 concomitantly with the deprotonation of the Schiff base (Engelhard et al., 1996). Similar experiments on SRII from *H. salinarum* (HsSRII) led to the same conclusions (Bergo et al., 2000). Resonance Raman (RR) spectroscopic data revealed strong hydrogen bonding interactions of the Schiff base in $\mathrm{NpSRII}_{500}$ and in $O_{535}$ which might be one parameter controlling the absorption maxima that are distinctly blue-shifted compared to the corresponding states of other bacterial rhodopsins (Gellini et al., 2000).

In this paper, RR data on the NpSRII photocycle intermediates are presented, which provide evidence of two spectrally distinct M spectral states. Surface enhanced resonance Raman (SERR) experiments indicate that an applied potential sensitively modifies the kinetics of the photocycle.

## MATERIALS AND METHODS

### Samples

Expression and purification of NpSRII is described previously (Hohenfeld et al., 1999; Shimono et al., 1997). The protein was dissolved in solutions containing 1% dodecylmaltoside, 12.5 mM $K_2SO_4$ and 12.5 mM phosphate buffer (pH 7.0). The NpSRII concentration was 30 $\mu$M and 0.1 $\mu$M in RR and SERR experiments, respectively.

### SERR experiments

RR and SERR spectra were measured at ambient temperature using a spectrograph (U1000) equipped with a liquid nitrogen cooled CCD camera (ISA, D-85360 Grasbrunn, Germany. Unless noted otherwise, the 413-nm excitation line of a $Kr^+$-laser (Coherent Innova 302, D-64807 Dieburg, Germany) was employed and the spectral resolution was 4 $cm^{-1}$ with an increment per data point of 0.53 $cm^{-1}$. Details of the experimental set-up are given elsewhere (Oellerich et al., 2002). In SERR experiments, the laser beam was focused onto the surface of a rotating Ag electrode that was placed into a home-built electrochemical cell containing NpSRII and detergent and the supporting electrolyte. Adsorption of the protein occurred spontaneously at open circuit. The electrochemical cell and the protocol for SERR-activation of the electrode is described elsewhere (Murgida and Hildebrandt, 2001a). All potentials cited in this work refer to the Ag/AgCl electrode.

### Time-resolved measurements

The laser beam used for probing the RR and SERR spectra also initiates the photocycle. The degree of photoconversion of the NpSRII during the residence time $\Delta t$ in the laser beam is given by

$$\frac{[p\mathrm{SRII}(\Delta t)]}{[p\mathrm{SRII}]_0} = \exp(-l_0 \Delta t). \quad (1)$$

The mean photochemical rate constant $l_0$ can be approximated by

$$l_0 = 0.48 \frac{\gamma \varepsilon(\lambda) P_\mathrm{L} \lambda}{r_\mathrm{L}^2}, \quad (2)$$

where $\gamma$ is the quantum yield of the primary photochemical process and $\varepsilon(\lambda)$ the extinction coefficient at the excitation wavelength $\lambda$ (Lohrmann and Stockburger, 1992). The laser power is denoted by $P_\mathrm{L}$, and $r_\mathrm{L}$ refers to the radius of the laser beam. For $\lambda = 413$ nm, the extinction coefficient of the parent state $\mathrm{NpSRII}_{500}$ is $\sim$15,000 $l \cdot mol^{-1} \cdot cm^{-1}$ (Chizhov et al., 1998). The quantum yield of the primary photoprocess has not yet been determined; however, for the formation of the long-lived intermediate $\mathrm{NpSRII}_{400}$, a value of 0.5 was published (Losi et al., 1999). Inserting these values as well as the laser beam radius of 40 $\mu$m, as defined according to Lohrmann and Stockburger (1992), into Eq. 9, one obtains

$$l_0 = 9 \times 10^5 \times P_\mathrm{L}, \quad (3)$$

where $P_\mathrm{L}$ is expressed in joules $\times$ s.

The residence time of the sample in the laser beam is given by

$$\Delta t = \frac{r_\mathrm{L}}{\pi r_\mathrm{c} \nu_0}, \quad (4)$$

where $r_\mathrm{c}$ and $\nu_0$ are the respective radius and the frequency of the rotating device that is a rotating cell and a rotating electrode in RR and SERR experiments, respectively.

To avoid quasi-photostationary conditions, the NpSRII molecules of the irradiated volume (RR) or surface (SERR) element must be allowed to relax to the parent state before entering the laser beam again. This condition requires that the minimal time interval between irradiation events is larger than the decay time of the longest-lived intermediate. For BR and HR, this requirement can be fulfilled by setting $\nu_0 \leq 50$ $s^{-1}$, whereas for NpSRII $\nu_0$ would have to be kept smaller than 1 $s^{-1}$. Such a slow rotation would drastically increase $\Delta t$ to $\sim$2 ms (Eq. 4), corresponding to a photoconversion parameter $l_0 \Delta t$ larger than one even at very low laser power (cf. Eq. 1). Under these conditions, a quasi-photostationary equilibrium between the parent state and the primary photoproduct would be formed in the laser beam, and the RR spectrum would include large contributions from intermediate states.

In our previous study on NpSRII (Gellini et al., 2000), we had chosen a compromise between a small photoconversion parameter and a small rotational frequency to probe the RR spectrum of the parent state, although accumulation of long-lived intermediates was inevitable. In the present work, we have employed a different approach by controlling the sample irradiation independent of the rotational frequency of the cell or the electrode. On the basis of a home-built multichannel pulse delay generator, a voltage-dependent intensity modulator (LM 202, Gsänger, D-82152 Planegg, Germany) is triggered via a pulse amplifier (LIV 8, Gsänger,

Planegg) to gate the exciting laser beam such that the irradiation interval corresponds to the rotational period ($1/\nu_0$) of the cell or the electrode and the dark interval is set equal to the time required for the parent state recovery. Thus, the ''fresh sample'' condition is fulfilled and formation of intermediates exclusively depends on $l_0\Delta t$. The smallest possible $\Delta t$ depends on the maximal $\nu_0$, which was 50 $s^{-1}$ for the rotating cell but, due to technical constraints, 5 $s^{-1}$ for the rotating electrode, corresponding to a minimal $\Delta t$ of 26 $\mu$s and 260 $\mu$s in RR and SERR experiments, respectively.

## RESULTS

### RR spectra

Fig. 1 displays the RR spectra of NpSRII in the frequency range between 1500 and 1660 $cm^{-1}$, which is dominated by the in-phase C=C stretching ($\nu_{C=C}$) of the conjugated retinal chain (Althaus et al., 1995). The frequency of this mode is correlated with the position of the first electronic transition ($\lambda_{max}$) of the retinal chromophore (Heyde et al., 1971). On the basis of this $\nu_{C=C}/\lambda_{max}$ relationship, it was possible to assign component spectra determined from the analysis of the RR spectra measured at different excitation conditions to individual species of the NpSRII photocycle (Gellini et al., 2000). A representative spectrum obtained with low laser power and a short residence time of the sample in the laser beam (corresponding to a small photoconversion parameter) is shown in Fig. 1 *A*. Under these conditions the parent state $NpSRII_{500}$ is the prevailing species in the probe volume. Moreover, the excitation wavelength of 514 nm that was employed in this experiment is in rigorous resonance with the electronic transition of $NpSRII_{500}$ (500 nm) such that its RR bands are preferentially enhanced over those of the intermediates. In this experiment, the fresh-sample condition is not completely fulfilled and long-lived species $N_{485}$ and $O_{535}$ were accumulated, whereas the contribution of $L_{495}$ formed during the residence time of the sample in the laser beam is considered to be negligibly small. Thus, the three C=C stretching modes at 1547, 1537, and 1555 $cm^{-1}$ are attributed to $NpSRII_{500}$, $N_{485}$, and $O_{535}$, respectively, according to the $\nu_{C=C}/\lambda_{max}$ relationship. Contributions from $M_{400}$ could not be observed under these conditions due to the lack of sufficient resonance enhancement.

The situation is different upon employing 413-nm excitation that allows preferential enhancement of the bands of $M_{400}$ compared to all other states of the NpSRII photocycle. Fig. 1 *B* shows such an RR spectrum obtained with a small photoconversion parameter, using the present approach, that satisfies the fresh-sample requirement. In this case, the dominant band is located at ~1568 $cm^{-1}$, which is expected for an unprotonated retinal Schiff base as in $M_{400}$ (Althaus et al., 1995) and also found for this intermediate in SRI of *H. salinarium* (Haupts et al., 1994). This band exhibits a clearly identifiable shoulder on the high frequency side at ~1580 $cm^{-1}$. The second strongest peak at ~1550 $cm^{-1}$ reveals an asymmetric shape indicating the involvement of more than

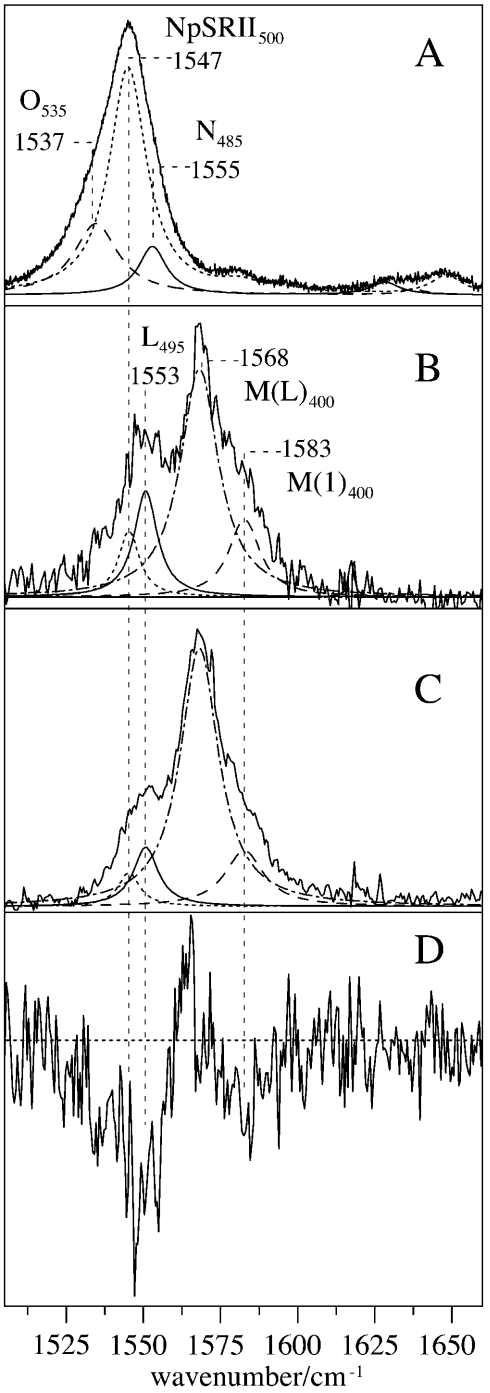


FIGURE 1 RR spectra of solubilized NpSRII in aqueous solution (pH 7.0) measured under different excitation conditions. (*A*) 514 nm, $\Delta t \cdot l_0 = 0.35$, $\Delta t = 10$ $\mu$s, $P_0 = 0.01$ W, nongated excitation; (*B*) 413 nm, $\Delta t \cdot l_0 = 0.234$, $\Delta t = 1300$ $\mu$s, $P_0 = 0.01$ W; gated excitation; (*C*) 413 nm, $\Delta t \cdot l_0 = 5.85$, $\Delta t = 260$ $\mu$s, $P_0 = 0.05$ W; gated excitation; (*D*) difference spectrum ''*C*'' minus ''*B*''. The dotted lines represent the component spectrum of $NpSRII_{500}$; in ''*A*'' the component spectra of the long-lived intermediates $O_{535}$ and $N_{485}$ are given by the dashed and solid lines, whereas in ''*B*'' and ''*C*'' the dashed-dotted, dashed, and solid lines represent the component spectra of $M(L)_{400}$, $M(1)_{400}$, and $L_{495}$, respectively.

one band in the frequency range of protonated retinal Schiff bases. The only candidates for these bands are the parent state $NpSRII_{500}$ and the intermediate $L_{495}$ that may be formed within $\Delta t$, whereas accumulation of long-lived intermediates (as in Fig. 1 *A*) can be ruled out. Thus, a band fitting analysis was carried out on the basis of four bands in this region. The spectral parameters of the C=C stretching of $NpSRII_{500}$ were adopted from our previous study (Gellini et al., 2000) and kept constant during the iteration. This analysis was extended to spectra obtained with different photoconversion parameters and, hence, different relative contributions of the various species to achieve a consistent global fit (Table 1). The C=C stretching frequency of $L_{495}$ is found to be somewhat lower than that of the $N_{485}$ intermediate, which is consistent with the slightly higher absorption maximum. The two high frequency modes at 1568 and 1583 $cm^{-1}$ are attributed to the C=C stretchings of two M-states, although the latter frequency is surprisingly high. However, an alternative assignment of the 1583 $cm^{-1}$ band to a second C=C stretching of one of the other NpSRII states can be ruled out since this band does not exhibit a constant intensity ratio with any of the remaining bands in this region. This is illustrated by the spectra in Fig. 1, *B* and *C* that were obtained with different laser power and residence times of sample in the laser beam. Thus, it is concluded that the 1583-$cm^{-1}$ originates from an additional M-like intermediate. The variation of the relative intensities of the individual bands with $\Delta t \cdot l_0$ is visualized by the difference spectrum (Fig. 1 *D*) and determined quantitatively by the band fitting analysis.

## Quantitative analysis

Upon 413-nm excitation, the RR bands of the M-species are predominantly enhanced compared to the parent state and those intermediates carrying a protonated Schiff base. Thus, the relative intensities $I_i$ of the C=C stretching modes do not reflect the relative concentrations $c_i$ of the underlying species *i*. Both quantities are related via

$$c_i = \frac{I_i}{\sigma_i}, \tag{5}$$

where $\sigma_i$ is a constant proportional to the RR cross section of the C=C stretching mode of the species *i*. These constants can be determined from the RR spectrum measured with $l_0\Delta t = 0.234$ (Fig. 1 *B*) on the basis of a previous kinetic study (Chizhov et al., 1998). These authors analyzed the photocycle in terms of *kinetically* distinguishable states ($P_j$) and evaluated the rate constants for the thermal decay processes (Table 1). Using these data as well as $l_0 = 9000\ s^{-1}$ derived from the excitations conditions of the RR experiment (Eqs. 3 and 4), it is possible to estimate the population of the individual states in the laser beam. The relative populations of $P_0$, $P_2$, $P_3$, and $P_4$ are calculated to be 0.795, 0.073, 0.095, and 0.037, respectively, whereas for all other states the population is <0.001. $P_0$, $P_2$, and $P_4$ are *spectrally* ''pure'' states and correspond to $NpSRII_{500}$, $L_{495}$, and $M_{400}$, respectively (Table 1). $P_3$ represents an ~1:3 mixture of an $L_{495}$ and an $M_{400}$ species that form a rapid equilibrium. In the transient UV-vis absorption spectra these species are spectrally not distinguishable from the $P_2$ ($L_{495}$) and $P_4$ ($M_{400}$) states. Also the present RR spectra do not provide any indication for spectral differences between the ''early'' ($P_2$) and the ''late'' ($P_3$) $L_{495}$ species, which both contribute to the 1553-$cm^{-1}$ band. Then, the total contribution of $L_{495}$ to the RR spectrum is the sum of $P_2$ and 25% of $P_3$. Conversely, the RR spectra reveal two C=C stretching modes attributable to two different $M_{400}$ species, which appear to be related to the ''early'' ($P_3$) $M_{400}$ and ''late'' ($P_4$) $M_{400}$, denoted as $M_L$ and $M_1$, respectively. Comparing relative intensities and calculated relative concentrations, the more intense 1568-$cm^{-1}$ and the weaker 1583-$cm^{-1}$ bands are assigned to $M_L$ and $M_1$, respectively. Following this assignment, the relative RR cross sections evaluated according to Eq. 5 are comparable for the C=C stretching modes of both $M_{400}$ species, which is consistent with the undistinguishable absorption maxima. The corresponding values for $NpSRII_{500}$ and $L_{495}$ differ substantially from each other, which is surprising in view of the similar absorption spectra. This discrepancy may partly be due to the larger error in the intensity determination of these relatively weak bands. Thus, the quantitative analysis of the spectra according to Eq. 5 may lead to an over- and underestimation of the relative concentrations of $NpSRII_{500}$ and $L_{495}$, respectively. Since this error is systematic, it will not affect the *changes* of the relative concentrations in the different spectra to which the discussion will be restricted.

Upon increasing the photoconversion parameter from 0.234 to 5.85 one would expect a substantial decrease of the parent state, whereas the experimentally determined decrease is only ~10% (Fig. 1 *C*, Table 2). These findings indicate

**TABLE 1 Kinetic and spectral parameters of NpSRII**

| Kinetic state* | $P_0$ | $P_1$ | $P_2$ | $P_3$ | | $P_4$ |
|---|---|---|---|---|---|---|
| Lifetime/s* | | $10^{-6}$ | $10^{-5}$ | $3{\cdot}10^{-5}$ | | $2{\cdot}10^{-3}$ |
| Species* | $NpSRII_{500}$ | $K_{510}$ | $L_{495}(1)$ | $L_{495}(2)$ (25%) | $M(L)_{400}$ (75%) | $M(1)_{400}$ |
| $\nu_{C=C}/cm^{-1}$ (RR) | 1546.8 | – | | 1553.3 | 1568.2 | 1582.7 |
| $\nu_{C=C}/cm^{-1}$ (SERR) | 1547.3 | – | | 1553.6 | 1568.7 | 1583.0 |
| $\sigma_i$† | 0.03 | – | | 0.36 | 1.00 | 0.68 |

*Data taken from Chizhov et al. (1998).
†Relative RR cross section as defined by Eq. 5.

**TABLE 2 Relative concentrations of the spectrally distinguishable states of the NpSRII photocycle**

| | Photoexcitation parameter* | | | Relative concentrations | | | | Concentration ratio |
|---|---|---|---|---|---|---|---|---|
| | $\Delta t/\mu s$ | $P_L/J\cdot s$ | $\Delta t \cdot I_0$ | $NpSRII_{500}$ | $L_{495}$ | $M(L)_{400}$ | $M(1)_{400}$ | $M_{400}(1)/M_{400}(2)$ |
| Calculated† | | | | | | | | |
| | 26 | 0.01 | 0.234 | 0.795 | 0.095 | 0.073 | 0.037 | 2.0 |
| | 260 | 0.001 | 0.234 | 0.795 | 0.112 | 0.017 | 0.176 | 0.10 |
| Experimental | | | | | | | | |
| SERR, open circuit | 260 | 0.001 | 0.234 | 0.37 | 0.11 | 0.38 | 0.14 | 2.7 |
| RR | 260 | 0.050 | 5.85 | 0.69 | 0.1 | 0.16 | 0.05 | 3.2 |
| SERR, open circuit | 1300 | 0.05 | 58.5 | 0.70 | 0.12 | 0.12 | 0.06 | 2.0 |
| SERR, open circuit | 260 | 0.01 | 2.34 | 0.68 | 0.08 | 0.16 | 0.08 | 2.0 |
| SERR, −0.4 V | 260 | 0.01 | 2.34 | 0.67 | 0.10 | 0.17 | 0.06 | 2.8 |

*Parameters are defined in Eqs. 3 and 4.
†Calculated according to a sequential reaction scheme using the photochemical rate constant defined in Eq. 2 and the thermal rate constants determined by Chizhov et al. (1998).

secondary photoreactions that lead to the back-conversion of intermediates to the parent state. This may particularly refer to the $M_{400}$ species since the exciting laser beam is in rigorous resonance with their electronic transitions. For $M(1)_{400}$ the photoconversion rate is evidently higher than that of $M(L)_{400}$ since the $M(L)_{400}/M(1)_{400}$ ratio has increased to ~3.25 from ~2.0 in the absence of secondary photoreactions. Note that this increase cannot be due to the thermal decay of $M(1)_{400}$ which occurs within 2 ms and, hence, can be neglected for a residence time of 260 $\mu$s in the probe beam.

## SERR spectroscopy

NpSRII adsorbs spontaneously to the bare silver electrode most likely via electrostatic interactions. Fig. 2 shows three time-resolved SERR spectra obtained under different excitation conditions compared with the SERR spectrum measured without gating the exciting laser beam (fresh-sample condition not fulfilled). All spectra are dominated by the 1568-$cm^{-1}$ band; however, they display substantial variations on the low- and high-frequency sides of this peak. The SERR spectra were analyzed using the spectral parameters of the RR bands as initial values. A consistent global fit required only minor alterations of these parameters. These adjustments are in the same range of those found in the simulation of RR and SERR spectra of other proteins (Oellerich et al., 2002). Furthermore, alterations of the contributions from the various species of NpSRII in the SERR measured under different excitation conditions demonstrate that the adsorbed photoreceptor has retained its activity and that the photocycle is not blocked.

The quantitative analysis, however, reveals differences in the photocycle kinetics compared to the protein in solution. The relative concentrations of the various species were evaluated using the relative cross sections determined in the RR experiment. This approach assumes that for each species the surface enhancement of the RR scattering is the same. For the thermal intermediates $L_{495}$, $M(L)_{400}$, and $M(1)_{400}$, this assumption appears to be justified since major changes in the distance or orientation of chromophore with respect to the electrode, which would affect the magnitude of the enhancement, are not very likely to occur when the retinal configuration (13-*cis*) is maintained. In $NpSRII_{500}$, the chromophore adopts an all-*trans* configuration, and the orientation of the molecular dipole moment relative to the electrode surface may be different. On the basis of the present results, it cannot be decided if a (possible) orientational difference has an impact on the surface enhancement. Regardless of this uncertainty, the *spectral* contributions of $NpSRII_{500}$ are generally very small and, hence, the determination of the relative concentration for this species is associated with a substantial inaccuracy. This is particularly true for the SERR spectrum measured with a residence time of 260 $\mu$s and a photoconversion parameter of 0.234 (Fig. 2 *D*). As it can already be seen by visual inspection of the spectrum, the intensity of C=C stretching of $NpSRII_{500}$ is very weak and the best fit corresponds to a relative concentration of only 0.37. Even taking into consideration an uncertainty in the intensity determination by a factor of 2.5, the concentration (0.60) will not approach the value that is predicted by a kinetic simulation (0.795) on the basis of the rate constants for NpSRII in solution (Table 2). Moreover, the predicted value represents the lower limit for the relative concentration of $NpSRII_{500}$ as photo-induced back-reactions from the intermediates to the parent state are not considered.

Even more striking are the deviations for the population of $M(L)_{400}$ as well as for the $M(L)_{400}/M(1)_{400}$ ratio that are predicted to be much smaller than the experimental values regardless of the true concentration of $NpSRII_{500}$ (Table 2). These findings cannot be rationalized in terms of an enhancement of the primary photochemical process, which would, at best, lead to a quasi-photostationary mixture of $NpSRII_{500}$ and $K_{510}$. Thus, it is concluded that the thermal reaction rates are altered in the adsorbed NpSRII.

An acceleration of the $L_{495}$ ($P_2$) decay (10 $\mu$s) cannot account for the large population of $M(L)_{400}$ and $M(1)_{400}$ during the residence time of the sample in the laser probe

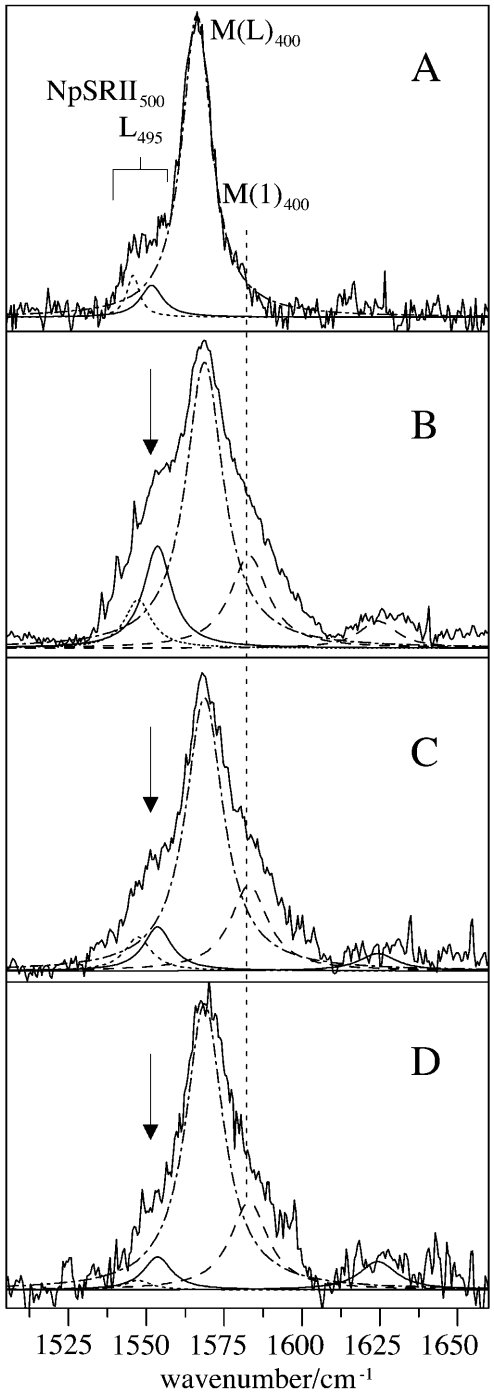


FIGURE 2 SERR spectra of immobilized NpSRII on the electrode at open circuit with 413 nm and different photoexcitation parameters. (*A*) $\Delta t \cdot I_0 = 70$, $\Delta t = 260$ $\mu$s, $P_0 = 0.06$ W; nongated excitation; (*B*) $\Delta t \cdot I_0 = 58.5$, $\Delta t = 1300$ $\mu$s, $P_0 = 0.05$ W, gated excitation; (*C*) $\Delta t \cdot I_0 = 2.34$, $\Delta t = 260$ $\mu$s, $P_0 = 0.01$ W, gated excitation; (*D*) $\Delta t \cdot I_0 = 0.234$, $\Delta t = 260$ $\mu$s, $P_0 = 0.001$ W, gated excitation. The dashed-dotted and dashed lines represent the component spectra of $M(L)_{400}$ and $M(1)_{400}$, respectively, and the component spectra of $NpSRII_{500}$ and $L_{495}$ are given by the dotted and solid lines, respectively.

beam (260 $\mu$s). Instead, the most probable explanation is that the decay times of $M(L)_{400}$ ($P_3$, 30 $\mu$s) and $M(1)_{400}$ ($P_4$, 2 ms) are drastically increased (>1 s) such that they become the rate-limiting steps of the photocycle, which is thus not completed before the sample is reirradiated by the probe beam. In this case, $M(L)_{400}$ and $M(1)_{400}$ are accumulated at the expense of $NpSRII_{500}$ as observed in the SERR spectrum. Note that a further increase of the dark time and a reduction of the laser power in the SERR experiments was not possible as such conditions required a substantial increase of the total measuring time which was in conflict with the insufficient long-term stability of the adsorbed protein.

SERR spectra measured with higher photoconversion parameters support the interpretation of increased decay time of the M-states in the adsorbed protein (Fig. 2, *B* and *C*). Regardless of the different residence times in the laser beam (260 $\mu$s and 1.3 ms), the spectra reveal essentially the same distribution between the parent and intermediate states implying that the lifetimes of $M_{400}$ states are distinctly longer than 1.3 ms. In both spectra, the total amount of both $M_{400}$ states is smaller by a factor of two than in the SERR spectrum measured with a photoconversion parameter of 0.234, indicating that, like in solution, these intermediates are photochemically reconverted to the parent state. This tendency is further enhanced upon omitting the dark intervals in the measurements (Fig. 2 *A*). In this spectrum also the contribution of $L_{495}$ is decreased by a factor of two and contributions from $M(1)_{400}$ cannot be detected anymore, whereas the parent state contribution is further increased.

SERR spectra measured at open circuit and 0.0 V (under otherwise identical conditions) are quite similar and include approximately the same relative contributions of $NpSRII_{500}$ and the intermediate states within the experimental accuracy (Fig. 3, *A* and *B*). Upon lowering the potential to −0.4 V, however, distinct changes are observed on the high- and low-frequency side of the 1568-$cm^{-1}$ band (Fig. 3 *C*) as demonstrated by a difference spectrum (Fig. 3 *D*). These changes correspond to an increase of $L_{495}$ and a decrease of $M(L)_{400}$ such that the $M(L)_{400}/M(1)_{400}$ ratio is raised from 2.0 at 0.0 V to 2.8 at −0.4 V. The relative contributions of the various species to the SERR spectrum measured at −0.4 V are in good agreement to those in the RR spectrum measured under similar excitation conditions ($\Delta t$ and $\Delta t \cdot I_0$).

## DISCUSSION

The crucial step in the molecular functioning of retinal proteins is the coupling of chromophore conformational transitions and those protein structural changes which guarantee unidirectionality for the transmembrane transport of ions in energy transducing proteins and induce the formation of the signaling state in sensory photoreceptors. For BR, evidence has been provided that this step occurs at the stage of the unprotonated retinal Schiff base and involves the transition between two M-states which have been

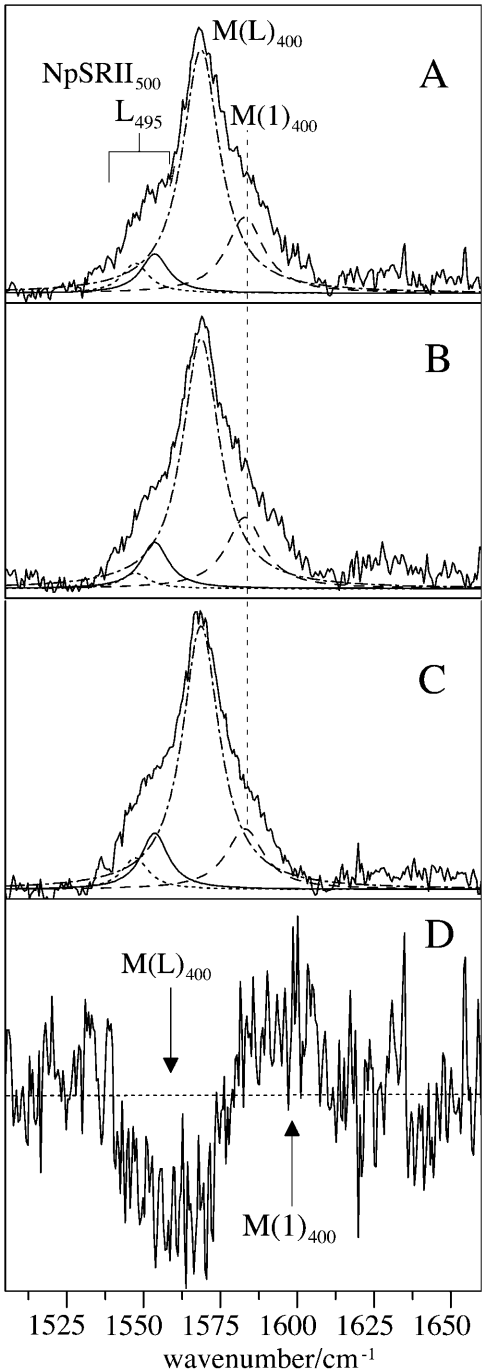


FIGURE 3 SERR spectra of immobilized NpSRII on the electrode measured with gated excitation at 413 nm ($\Delta t \cdot I_0 = 2.34$, $\Delta t = 260$ $\mu$s, $P_0 = 0.010$ W) at (*A*) open circuit, (*B*) 0.0 V, and (*C*) −0.4 V. The dashed-dotted and dashed lines represent the component spectra of $M(L)_{400}$ and $M(1)_{400}$, respectively, and the component spectra of $NpSRII_{500}$ and $L_{495}$ are given by the dotted and solid lines, respectively. (*D*) is the difference spectrum "*B*" minus "*C*".

denoted M1 and M2 (Váró and Lanyi, 1990; Ormos, 1991). M1 is preceded by protein states comprising fast L → M equilibria (Chizhov et al., 1996). So far, all attempts to identify different M-states by RR spectroscopy failed since either the lifetime of the late M-state is too short or the chromophore structure is essentially the same in the different M-states. Thus, the results obtained for NpSRII in this work represent the first example for M-states that exhibit different RR spectra.

The transition from the early $M(L)_{400}$ to the late $M(1)_{400}$ in NpSRII is associated with an upshift of the C=C stretching frequency by ~15 $cm^{-1}$ to an unusually high value of 1583 $cm^{-1}$. Unlike for protonated retinal Schiff bases, little is known about parameters that may affect the RR spectra of the unprotonated chromophores. Early RR studies on model compounds in solution have shown that polarity and hydrophobicity of the solvent influence the C=C stretching frequency (Heyde et al., 1971). Although a unique relationship with the dielectric constant of the solvent is not evident from the experimental data, at least for all-*trans* retinals the highest C=C stretching frequencies (>1580 $cm^{-1}$) are observed in nonpolar solvents. We conclude, therefore, that the transition from $M(L)_{400}$ to $M(1)_{400}$ is linked to structural changes in the retinal binding pocket generating a largely hydrophobic environment in which, similar as in solution, the polyene chain adopts a fully relaxed conformation. This conclusion is corroborated by time-resolved IR spectroscopic experiments, which have shown variations of the amide bands indicating changes of the protein secondary structure (F. Siebert, personal communication, Universität Freiburg, 2002).

A largely nonpolar environment would stabilize an unprotonated Schiff base and thus may account for the relatively long lifetime of this M-state compared to that of BR. The different characteristics of the formation and decay of the late M-states in NpSRII and BR can be, at least in part, rationalized on the basis of the three-dimensional structures available for the parent states of both proteins. The retinal binding pockets of $BR_{570}$ and $NpSRII_{500}$ differ with respect to the arrangement of charged and polar amino acid residues (Luecke et al., 2001; Luecke et al., 1999; Royant et al., 2001). Specifically, Arg-72 that weakens the protonated Schiff base interactions with the counterion in $BR_{570}$ is displaced from the Schiff base in $NpSRII_{500}$. This reorientation (Ren et al., 2001) as well as the substitution of polar side chains by nonpolar amino acids (Hayashi et al., 2001), which have been suggested to be the main origin for the blue-shifted absorption maximum in NpSRII, reduces the polarity of the binding pocket already in the parent state. Protein structural changes during the $M(L)_{400} \rightarrow M(1)_{400}$ transition in NpSRII may further enhance this effect to afford a particularly nonpolar environment for the retinal that gives rise to the unusual high C=C stretching frequency.

Upon adsorption on the metal electrode, NpSRII remains photoactive such that it runs reversibly through the photocycle. There are no indications for intermediate states that are different from those of the photocycle in solution. The C=C stretching vibrations used for identification of the parent and intermediate states are very similar for the solubilized and

immobilized photoreceptor. Adsorption-induced frequency differences are as small as for proteins (e.g., cytochrome *c*) for which preservation of the native structure in the adsorbed state has been proven independently (Oellerich et al., 2002; Murgida and Hildebrandt, 2001a). This conclusion does not rule out local structural changes in the binding domain, which would be invisible in the SERR experiments.

In the potential range of the present SERR study, i.e., above the potential of zero charge ($E_{PZC} \approx -0.9$ V), the Ag electrode is covered with specifically adsorbed anions that overcompensate the positive charge of the metal and hence favor electrostatic binding of proteins that exhibit a cationic region on the surface. This is also true for an electrode kept at open circuit for which the charge distribution is similar to an electrode at 0.0 V (Henglein and Lilie, 1981).

The crystal structure of NpSRII reveals a positively charged patch on the cytoplasmic side of helix F, which presumably serves as the interaction domain for the transducer protein NpHtrII (Royant et al., 2001). Since there are no other positively charged regions on the cytoplasmic or extracellular sides of the protein, this domain represents also the preferred site for electrostatic binding to the electrode. Thus, it is very likely that NpSRII adsorbs in a uniform orientation with the cytoplasmic side being in contact with the electrode. In this orientation, the retinal chromophore is separated from the metal surface by ~30 Å.

The main difference between the solubilized and immobilized NpSRII refers to the photocycle kinetics. At 0.0 V and open circuit, the thermal decays of the M-states are drastically slowed down. Since the subsequent intermediate $N_{485}$ exhibits the same chromophore configuration as $M(L)_{400}$ and $M(1)_{400}$, the rate-limiting steps must be associated with conformational changes in the protein matrix. These structural changes include alterations of the secondary structure that require the rupture and formation of hydrogen bonds and proton translocations that eventually lead to the reprotonation of the Schiff base in $N_{485}$. Thus, the M-state decays involve the movement of protons, which can be sensitively affected by electric fields as has been shown for the redox-linked reorganization of the hydrogen bonding network in cytochrome *c* (Murgida and Hildebrandt, 2001b). In that case, the electric field experienced by the immobilized protein raises the activation barrier for the underlying proton transfer steps (Murgida and Hildebrandt, 2002), which consequently are slowed down significantly and become rate-limiting for the interfacial redox process. The lowest rate ($<5\ s^{-1}$) is observed for proteins adsorbed directly in the electrical double layer (Lecomte et al., 1999) where the electric field is particularly high. As in this latter case, also NpSRII is bound to the layer of chemisorbed anions on the electrode presumably via the cationic domain on the cytoplasmic side of the protein (see above). Thus, the interfacial potential drop and the electric field strength in the retinal binding pocket are most likely comparable to that for cytochrome *c* (Lecomte et al., 1999; Murgida and Hildebrandt, 2001a). Hence, we conclude that also the ultimate origin for the retardation of the M-state decays in NpSRII is an electric-field induced increase of the energy barrier of proton transfer steps that are associated with rearrangements of the hydrogen bond network required for the conformational transitions of $M(L)_{400}$ and $M(1)_{400}$.

The magnitude of the electric field depends on the distance of the protein to the electrode that we have varied in our previous studies on cytochromes (Murgida and Hildebrandt, 2001a, 2001b, 2002; Simaan et al., 2002), and on the interfacial charge distribution that can be altered by changing the electrode potential (Lecomte et al., 1999). Shifting the potential $E$ to negative values decreases the field strength since the difference $(E - E_{PZC})$ is reduced. In fact, at −0.4 V the distribution among the various states of NpSRII differs from that measured at 0.0 V and at open circuit, particularly with respect to the $M_L/M_1$ ratio. Moreover, the distribution is very similar to that found for the solubilized NpSRII under the same excitation conditions. These findings imply that at −0.4 V the electric field strength is not sufficient to affect the proton transfer kinetics substantially.

Extensive studies on the photocycle kinetics of BR have shown that the regeneration of the parent state is substantially slowed down under the influence of electric fields (Bamberg and Fahr, 1980; Dancshazy et al., 1983; Westerhoff and Dancshazy, 1984; Groma et al., 1984; Braun et al., 1988; Nagel et al., 1998). These results were attributed to the fact that the transmembrane proton transport starts with the deprotonation of the retinal Schiff base, i.e., the formation of the M-state. More detailed information has been obtained by Bamberg and co-workers who succeeded in reconstituting BR in membranes with a uniform orientation (Geibel et al., 2001). The authors demonstrated that at transmembrane potentials that prohibit proton pumping, specifically the decays of the early and late M-states are slowed down and thus opening a new pathway for the transformation to the parent state that is not associated with transmembrane proton transfer. Also for pSRI, an electric-field dependent retardation of the M-state decay was observed (Manor et al., 1988).

These findings appear to be strongly related to the present results on NpSRII although its primary function is not proton pumping. However, also, the conformational changes associated with the formation of the signaling state include proton transfer steps, and even proton pump activity cannot be ruled out. Thus, it is very likely that the electric-field dependence of the M-state transitions is a common characteristic of (archae)bacterial retinal proteins. For ion pumping proteins, the functional importance of these effects is immediately evident inasmuch as they may constitute a feedback control for the generation of ion gradients that are utilized to drive ATP synthesis. Taking into account the results of our previous studies on cytochrome *c* (Murgida and Hildebrandt, 2001a, 2001b, 2002), the molecular basis

for such a mechanism may be attributed to the electric-field induced increase of the activation barrier for proton translocations. The implication of these findings for the sensor NpSRII which experiences in its natural host *N. pharaonis* a membrane potential of $\sim -250$ mV (Wittenberg, 1995) has to be elucidated.

## REFERENCES


Althaus, T., W. Eisfeld, R. Lohrmann, and M. Stockburger. 1995. Application of Raman spectroscopy to retinal proteins. *Isr. J. Chem.* 35:227–251.

Bamberg, E., and A. Fahr. 1980. Photocurrents induced on black lipid membranes by purple membranes: a method for reconstitution and a kinetic study of the photocurrents. *Ann. N. Y. Acad. Sci.* 358:324–327.

Bergo, V., E. N. Spudich, K. L. Scott, J. L. Spudich, and K. J. Rothschild. 2000. FTIR analysis of the $SII_{540}$ intermediate of sensory rhodopsin II: Asp73 is the Schiff base proton acceptor. *Biochemistry.* 39:2823–2830.

Blanck, A., D. Oesterhelt, E. Ferrando, E. S. Schegk, and F. Lottspeich. 1989. Primary structure of sensory rhodopsin I, a prokaryotic photoreceptor. *EMBO J.* 8:3963–3971.

Braun, D., N. A. Dencher, A. Fahr, M. Lindau, and M. P. Heyn. 1988. Nonlinear voltage dependence of the light-driven proton pump current of bacteriorhodopsin. *Biophys. J.* 53:617–621.

Chizhov, I., D. S. Chernavskii, M. Engelhard, K. H. Müller, B. V. Zubov, and B. Hess. 1996. Spectrally silent transitions in the bacteriorhodopsin photocycle. *Biophys. J.* 71:2329–2345.

Chizhov, I., G. Schmies, R. Seidel, J. R. Sydor, B. Lüttenberg, and M. Engelhard. 1998. The photophobic receptor from *Natronobacterium pharaonis*: temperature and pH dependencies of the photocycle of sensory rhodopsin II. *Biophys. J.* 75:999–1009.

Dancshazy, Z., S. L. Helgerson, and W. Stoeckenius. 1983. Coupling between the bacteriorhodopsin photocycle kinetics and the protonmotive force. 1. Single flash measurements in *Halobacterium halobium* cells. *Photobiochem. Photobiophys.* 5:347–357.

Engelhard, M., B. Scharf, and F. Siebert. 1996. Protonation changes during the photocycle of sensory rhodopsin II from *Natronobacterium pharaonis*. *FEBS Lett.* 395:195–198.

Geibel, S., T. Friedrich, P. Ormos, P. G. Wood, G. Nagel, and E. Bamberg. 2001. The voltage-dependent proton pumping in bacteriorhodopsin is characterized by optoelectric behavior. *Biophys. J.* 81:2059–2068.

Gellini, C., B. Lüttenberg, J. Sydor, M. Engelhard, and P. Hildebrandt. 2000. Resonance Raman spectroscopy of sensory rhodopsin II from *Natronobacterium pharaonis*. *FEBS Lett.* 472:263–266.

Groma, G. I., S. L. Helgerson, P. K. Wolber, D. Beece, Z. Dancshazy, L. Keszthelyi, and W. Stoeckenius. 1984. Coupling between the bacteriorhodopsin photocycle kinetics and the protonmotive force in *Halobacterium halobium* cell envelope vesicles. 2. Quantitation and preliminary modeling of the M $\rightarrow$ BR reactions. *Biophys. J.* 45:985–992.

Haupts, U., W. Eisfeld, M. Stockburger, and D. Oesterhelt. 1994. Sensory rhodopsin I photocycle intermediate $SRI_{380}$ contains 13-*cis* retinal bound via an unprotonated Schiff base. *FEBS Lett.* 356:25–29.

Hayashi, S., E. Tajkhorshid, E. Pebay-Peyroula, A. Royant, E. M. Landau, J. Navarro, and K. Schulten. 2001. Structural determinants of spectral tuning in retinal proteins-bacteriorhodopsin vs sensory rhodopsin II. *J. Phys. Chem. B.* 105:10124–10131.

Henglein, A., and J. Lilie. 1981. Storage of electrons in aqueous solution: the rates of chemical charging and discharging the colloidal silver microelectrode. *J. Am. Chem. Soc.* 103:1059–1066.

Heyde, M. E., D. Gill, R. G. Kipponen, and L. Rimai. 1971. Raman spectra of Schiff bases of retinal (models of visual photoreceptors). *J. Am. Chem. Soc.* 93:6776–6780.

Hirayama, J., Y. Imamoto, Y. Shichida, N. Kamo, H. Tomioka, and T. Yoshizawa. 1992. Photocycle of phoborhodopsin from haloalkaliphilic bacterium (*Natronobacterium pharaonis*) studied by low-temperature spectrophotometry. *Biochemistry.* 31:2093–2098.

Hohenfeld, I. P., A. A. Wegener, and M. Engelhard. 1999. Purification of histidine tagged bacteriorhodopsin, *pharaonis* halorhodopsin and *pharaonis* sensory rhodopsin II functionally expressed in *Escherichia coli*. *FEBS Lett.* 442:198–202.

Imamoto, Y., Y. Shichida, J. Hirayama, H. Tomioka, N. Kamo, and T. Yoshizawa. 1992. Nanosecond laser photolysis of phoborhodopsin: From *Natronobacterium pharaonis* appearance of KL and L intermediates in the photocycle at room temperature. *Photochem. Photobiol.* 56:1129–1134.

Kandori, H., K. Shimono, Y. Sudo, M. Iwamoto, Y. Shichida, and N. Kamo. 2001. Structural changes of pharaonis phoborhodopsin upon photoisomerization of the retinal chromophore: infrared spectral comparison with bacteriorhodopsin. *Biochemistry.* 40:9238–9246.

Lanyi, J. K., and G. Váró. 1995. The photocycles of bacteriorhodopsin. *Isr. J. Chem.* 35:365–385.

Lecomte, S., P. Hildebrandt, and T. Soulimane. 1999. Dynamics of the heterogeneous electron-transfer reaction of cytochrome $c_{552}$ from *Thermus thermophilus*. A time-resolved surface-enhanced resonance Raman spectroscopic study. *J. Phys. Chem. B.* 103:10053–10064.

Lohrmann, R., and M. Stockburger. 1992. Time-resolved resonance Raman studies of bacteriorhodopsin and its intermediates $K_{590}$ and $L_{550}$: biological implications. *J. Raman Spectrosc.* 23:575–583.

Losi, A., A. A. Wegener, M. Engelhard, W. Gärtner, and S. E. Braslavsky. 1999. Time-resolved absorption and photothermal measurements with recombinant sensory rhodopsin II from *Natronobacterium pharaonis*. *Biophys. J.* 77:3277–3286.

Luecke, H., B. Schobert, J. K. Lanyi, E. N. Spudich, and J. L. Spudich. 2001. Crystal structure of sensory rhodopsin II at 2.4 angstroms: insights into color tuning and transducer interaction. *Science.* 293:1499–1503.

Luecke, H., B. Schobert, H. T. Richter, J. P. Cartailler, and J. K. Lanyi. 1999. Structure of bacteriorhodopsin at 1.55 Å resolution. *J. Mol. Biol.* 291:899–911.

Manor, D., C. A. Hasselbacher, and J. L. Spudich. 1988. Membrane-potential modulates photocycling rates of bacterial rhodopsins. *Biochemistry.* 27:5843–5848.

Miyazaki, M., J. Hirayama, M. Hayakawa, and N. Kamo. 1992. Flash photolysis study on pharaonis phoborhodopsin from a haloalkaliphilic bacterium (*Natronobacterium pharaonis*). *Biochim. Biophys. Acta.* 1140:22–29.

Murgida, D. H., and P. Hildebrandt. 2001a. Heterogeneous electron transfer of cytochrome *c* on coated silver electrodes. Electric field effects on structure and redox potential. *J. Phys. Chem. B.* 105:1578–1586.

Murgida, D. H., and P. Hildebrandt. 2001b. Proton-coupled electron transfer of cytochrome *c*. *J. Am. Chem. Soc.* 123:4062–4068.

Murgida, D. H., and P. Hildebrandt. 2002. Electrostatic-field dependent activation energies control biological electron transfer. *J. Phys. Chem. B.* 106:12814–12819.

Nagel, G., B. Kelety, B. Möckel, G Büldt, and E. Bamberg. 1998. Voltage dependence of proton pumping by bacteriorhodopsin is regulated by the voltage-sensitive ratio $M_1$ to $M_2$. *Biophys. J.* 74:403–412.

Oellerich, S., H. Wackerbarth, and P. Hildebrandt. 2002. Spectroscopic characterization of nonnative conformational states of cytochrome *c*. *J. Phys. Chem. B.* 106:6566–6580.

Ormos, P. 1991. Infrared spectroscopic demonstration of a conformational change in bacteriorhodopsin involved in proton pumping. *Proc. Natl. Acad. Sci. USA.* 88:473–477.

Ren, L., C. H. Martin, K. J. Wise, N. B. Gillespie, H. Luecke, J. K. Lanyi, J. L. Spudich, and R. R. Birge. 2001. Molecular mechanism of spectral tuning in sensory rhodopsin II. *Biochemistry.* 40:13906–13914.

Royant, A., P. Nollert, R. Neutze, E. M. Landau, E. Pebay-Peyroula, and J. Navarro. 2001. X-ray structure of sensory rhodopsin II at 2.1-Å resolution. *Proc. Natl. Acad. Sci. USA.* 98:10131–10136.

Schäfer, G., M. Engelhard, and V. Müller. 1999. Bioenergetics of the archaea. *Microbiol. Mol. Biol. Rev.* 63:570–620.

Scharf, B., B. Pevec, B. Hess, and M. Engelhard. 1992. Biochemical and photochemical properties of the photophobic receptors from *Halobacterium halobium* and *Natronobacterium pharaonis*. *Eur. J. Biochem.* 206:359–366.

Schmies, G., M. Engelhard, P. G. Wood, G. Nagel, and E. Bamberg. 2001. Electrophysiological characterization of specific interactions between bacterial sensory rhodopsins and their transducers. *Proc. Natl. Acad. Sci. USA.* 98:1555–1559.

Seidel, R., B. Scharf, M. Gautel, K. Kleine, D. Oesterhelt, and M. Engelhard. 1995. The primary structure of sensory rhodopsin II: a member of an additional retinal protein subgroup is coexpressed with its transducer, the halobacterial transducer of rhodopsin II. *Proc. Natl. Acad. Sci. USA.* 92:3036–3040.

Shimono, K., M. Iwamoto, M. Sumi, and N. Kamo. 1997. Functional expression of pharaonis phoborhodopsin in *Escherichia coli*. *FEBS Lett.* 420:54–56.

Simaan, A. J., D. H. Murgida, and P. Hildebrandt. 2002. Active site structure and dynamics of cytochrome $c_3$ from *Desulfovibrio gigas* immobilized on electrodes. *Biopolymers.* 67:331–334.

Spudich, J. L. 1998. Variations on a molecular switch: transport and sensory signalling by archaeal rhodopsins. *Mol. Microbiol.* 28:1051–1058.

Spudich, J. L., and H. Luecke. 2002. Sensory rhodopsin II: functional insights from structure. *Curr. Opin. Struct. Biol.* 12:540–546.

Váró, G., and J. K. Lanyi. 1990. Protonation and deprotonation of the M, N, and O intermediates during the bacteriorhodopsin photocycle. *Biochemistry.* 29:6858–6865.

Wegener, A. A., I. Chizhov, M. Engelhard, and H. J. Steinhoff. 2000. Time-resolved detection of transient movement of helix F in spin-labelled pharaonis sensory rhodopsin II. *J. Mol. Biol.* 301:881–891.

Westerhoff, H. V., and Z. Dancshazy. 1984. Keeping a light-driven proton pump under control. *Trends Biochem. Sci.* 9:112–117.

Wittenberg, R. 1995. Charakterisierung der Elektronentransportkette und Untersuchungen zur Bioenergetik in *Natronobacterium pharaonis*. Ruhr-Universität, Bochum, Germany.

Zhang, W. S., A. Brooun, M. M. Mueller, and M. Alam. 1996. The primary structures of the archaeon *Halobacterium salinarium* blue light receptor sensory rhodopsin II and its transducer, a methyl-accepting protein. *Proc. Natl. Acad. Sci. USA.* 93:8230–8235.